Published in final edited form as:
Neuroimage. 2013 October 1; 79: . doi:10.1016/j.neuroimage.2013.04.062.

Frequency specific interactions of MEG resting state activity within and across brain networks as revealed by the Multivariate Interaction Measure

L. Marzetti[1,2], **S. Della Penna**[1,2], **AZ. Snyder**[3,4], **V. Pizzella**[1,2], **G. Nolte**[5], **F. de Pasquale**[1,2], **GL. Romani**[1,2], and **M Corbetta**[1,2,3,4]

[1]Department of Neuroscience and Imaging, "G. d'Annunzio" University Chieti-Pescara, Chieti, Italy

[2]Institute for Advanced Biomedical Technologies, "G. d'Annunzio" University Foundation, Chieti, Italy

[3]Department of Neurology, Washington University, St. Louis, Missouri

[4]Departments of Radiology, Washington University, St. Louis, Missouri

[5]Department of Neurophysiology and Pathophysiology, University Medical Center Hamburg-Eppendorf, Hamburg, Germany

Abstract

Resting state networks (RSNs) are sets of brain regions exhibiting temporally coherent activity fluctuations in the absence of imposed task structure. RSNs have been extensively studied with fMRI in the infra-slow frequency range (nominally $< 10^{-1}$ Hz). The topography of fMRI RSNs reflects stationary temporal correlation over minutes. However, neuronal communication occurs on a much faster time scale, at frequencies nominally in the range of $10^0 – 10^2$ Hz. We examined phase-shifted interactions in the delta (2–3.5 Hz), theta (4–7 Hz), alpha (8–12 Hz) and beta (13–30 Hz) frequency bands of resting-state source space MEG signals. These analyses were conducted between nodes of the dorsal attention network (DAN), one of the most robust RSNs, and between the DAN and other networks. Phase shifted interactions were mapped by the Multivariate Interaction Measure (MIM), a measure of true interaction constructed from the maximization of imaginary coherency in the virtual channels comprised of voxel signals in source space. Non zero-phase interactions occurred between homologous left and right hemisphere regions of the DAN in the delta and alpha frequency bands. Even stronger non zero-phase interactions were detected between networks. Visual regions bilaterally showed phase-shifted interactions in the alpha band with regions of the DAN. Bilateral somatomotor regions interacted with DAN nodes in the beta band. These results demonstrate the existence of consistent, frequency specific phase-shifted interactions on a millisecond time scale between cortical regions within RSN as well as across RSNs.

Corresponding author with complete address, including an email address: Laura Marzetti, PhD, Department of Neuroscience and Imaging, "G. d'Annunzio" University Chieti-Pescara, and Institute for Advanced Biomedical Technologies, "G. d'Annunzio" University Foundation, Via dei Vestini, 66013 Chieti, Italy. Tel. 0039-0871-3556942, Fax. 0039-0871-3556930, lmarzetti@unich.it.

Keywords

imaginary coherence; magnetoencephalography; resting state networks

INTRODUCTION

Following the seminal work of Biswal et al., (1995), resting state networks (RSNs) are defined as networks of brain regions that exhibit temporally coherent activity fluctuations in the absence of identifiable temporal structure (tasks, stimuli or endogenously generated events). RSNs have been mapped over the entire cerebral cortex (Buckner et al., 2011; Doucet et al., 2011; Yeo et al., 2011). Each RSN has been associated with specific cognitive processes (Cole et al., 2010; Deco & Corbetta, 2010; Fox & Raichle, 2007; Laird et al., 2011). Most of what is currently known about RSNs derives from resting state functional magnetic resonance imaging (fMRI), and, consequently, signals in the infra slow frequency range (nominally less than 0.1 Hz).

Much less is known concerning RSNs on a time scale relevant to behavior, i.e., frequencies in the 1 – 100 Hz range. Electroencephalography (EEG) and magnetoencephalography (MEG) (Cohen, 1972; Hämäläinen et al., 1993; Hari & Salmelin, 2012) are non-invasive techniques with millisecond temporal resolution, well suited to the study of neuronal activity in this frequency range. EEG and MEG record the activity of “coalitions of neurons” (Crick and Koch, 2003) that give rise to macroscopic magnetic fields and potential differences at the scalp. Observed oscillations in these fields are generated by phase-synchronous activity in large assemblies of neurons. These oscillations provide a basis for defining functional brain networks (for a review see Varela et al., 2001 and Siegel et al., 2012). Indeed, coherent neuronal activity has been hypothesized to serve as a mechanism for neuronal communication (Fries, 2005). Invasively recorded coherent multi-unit activity and local field potentials (Womelsdorf et al., 2007) as well as non-invasively recorded scalp potentials (EEG) (Tallon-Baudry et al., 1996) and MEG (Gross et al., 2006; Siegel et al. 2008) signals have been extensively described. However, the great preponderance of this work concerns transient coherence induced by task- or stimulus-related events, e.g., (Siegel et al., 2008).

The MEG correlates of fMRI RSNs have been recently reported (Brookes et al., 2011a; Brookes et al., 2011b; de Pasquale et al., 2010; de Pasquale et al., 2012). These studies describe correlations in band-limited power envelopes at infra-slow frequencies i.e., on a time scale similar to that of fMRI. However, MEG and EEG allow the estimation of functional connectivity metrics at much faster time scales, i.e., in the 1–100 Hz range. Indeed, it is possible to investigate neuronal communication within and between RSNs by focusing on the phase relations of oscillations in (possibly) interacting neuronal pools, with the additional possibility of examining specific brain rhythms, that is particular frequency ranges.

To this end, we reconstruct source-space MEG signals and compute the Multivariate Interaction Measure (MIM) (Ewald et al., 2012). MIM measures the interaction between vector signals based on complex coherence (correlation in the frequency domain). MIM is based on the maximization of the imaginary part of coherence between MEG source space signals, which implies robustness to mixing distortions (Nolte et al., 2004; Pascual-Marqui RD, 2007; Schoeffelen & Gross, 2009; Sekihara et al., 2011). Thus, significant non-zero MIM values cannot be generated by independent sources. Moreover, the maximization of imaginary part of coherence between subspaces leads, in general, to an increase in signal to noise ratio by construction and to the potential observation of interactions otherwise embedded into noise (Ewald et al., 2012).

We previously investigated MEG RSNs using correlation of band-limited power (BLP) (de Pasquale et al., 2010; de Pasquale et al., 2012). In those analyses, RSN functional connectivity was found only intra-hemispherically unless non-stationarity of the BLP correlation was explicitly taken into account. Here, we assume stationarity but we take into account systematic temporal delays in signal propagation. We investigate within- and between-RSN interactions with special attention to the question of inter-hemispheric functional connectivity. We focus our analysis on the dorsal attention network (DAN), one of the most robust and well-defined fMRI RSNs. The DAN characteristically is recruited by tasks that require the endogenous control of spatial attention (Corbetta and Shulman, 2002), is highly symmetric and therefore is well suited to investigating the question of inter-hemispheric functional connectivity. Moreover, the DAN interacts with other functional networks, especially the somatomotor and visual systems, and plays a central role in linking relevant sensory stimuli to motor responses (Corbetta and Shulman, 2002). This functional role makes the DAN well suited to investigation of the coupling between networks in the resting state.

METHODS

1. Subjects, Procedures, and Acquisition

The present data were acquired in 12 healthy young adult subjects (mean age 29 ± 6 years, five females, all right handed; same dataset described in de Pasquale et al., 2010 and 2012). Each subject contributed two 5 min resting state MEG runs during which they were instructed to maintain fixation on a visual crosshair. MEG was recorded using the 165-channel MEG system installed at the University of Chieti (Della Penna et al., 2000). This system includes 153 dc SQUID integrated magnetometers arranged on a helmet covering the whole head plus 12 reference channels. Two electrical channels simultaneously recorded electrocardiogram (ECG) and electrooculogram (EOG) signals for use in artifact rejection. All signals were band-pass filtered at 0.16–250 Hz and digitized at 1 kHz. The position of the subject's head with respect to the sensors was determined by five coils placed on the scalp recorded before and after each MEG run. The coil positions were digitized by means of a 3D digitizer (3Space Fastrak; Polhemus), together with anatomical landmarks (left and right preauricular and nasion) defining a head coordinate system. Anatomical images were acquired using a sagittal magnetization prepared rapid acquisition gradient echo T1-weighted sequence (MP-RAGE; Siemens Vision scanner 1.5 T; TR = 9.7 s, echo time TE = 4 ms, alpha = 12°, inversion time = 1200 ms, voxel size = 1×1×1.25 mm^3).

2. MEG Source Space Signal Estimation

After downsampling to 341 Hz, the recorded data were preprocessed using an independent components analysis (ICA) based algorithm. In brief, the algorithm automatically classifies the ICs and identifies artifactual components and components of brain origin. Typically, ICA based pipelines rely on the subtraction of artifactual ICs from MEG recordings to increase the signal-to-noise ratio. An alternative strategy is that of reconstructing MEG signals by recombining the ICs of brain origin either in signal or in source space (Mantini et al., 2011). The latter approach is pursued in this work. ICs classified as brain components by the fastICA algorithm with deflation approach (see Mantini et al., 2011 for details on the classification scheme), typically 10 to 15 in number, are input to a weighted minimum-norm least squares (WMNLS) linear inverse (Fuchs et al., 1999; Hämäläinen & Ilmoniemi, 1994) implemented in Curry 6.0 (Neuroscan). Source-space current is reconstructed on a Cartesian 3D grid bounded by the subject brain volume as derived from segmentation of individual magnetic resonance images (Curry 6.0 - Neuroscan). Source-space current corresponding to the i-th IC is computed as

$$\hat{s}_i = W^{-1}L^T(LW^{-1}L^T + \nu_i I)^{\dagger} a_i, \quad (1)$$

where a_i is the i-th IC topography, L is the lead-field matrix for the MEG forward problem, W is a diagonal weighting matrix, the elements of which are defined as $w_{jj} = |L_j|$ (with L_j being the three field components for unit dipoles in three directions at the j-th voxel). The symbol $|\cdot|$ denotes the Frobenius norm); ν_i is the regularization parameter for each IC and I is the identity matrix. The superscripts −1, T and † indicate matrix inverse, transpose and pseudoinverse, respectively.

As the ICs are typically characterized by relatively simple source configurations, the localization of their associated source-space maps within the cortex can potentially provide high accuracy in the detection of source generators (Tsai et al., 2006). Approaches differ for the choice of the regularization parameter. In WMNLs, this parameter is set on the basis of the deviation between the measured data and the forward calculated data using the chi-squared criterion, which relies on the assumption that signal power is comparable to noise in the data. In separately localizing independent component topographies, the regularization parameter λ_I is set for each IC rather than for the whole recording, thus proving an individualized estimate of the signal to noise ratio. Further details on ICA classification and source localization steps are given in (Mantini et al., 2011) and (de Pasquale et al., 2010).

Once the topographies have been projected onto the source space, the activity at each voxel and each time sample, $[\hat{q}_{jx}(t)\ \hat{q}_{jy}(t)\ \hat{q}_{jz}(t)]$, was obtained as a linear combination of IC time courses weighted by their related source space map. A dimensionality reduction step then was performed via principal component analysis (PCA). Of the three PCA eigenvalues ($\lambda_1 > \lambda_2 > \lambda_3$), the magnitude of λ_3 is systematically much smaller than that of λ_1. Thus, in our data, over all subjects, in 99% of the voxels $\lambda_3/\lambda_1 \leq 0.1$. However, λ_2 magnitude is comparable with that of λ_1. Thus, over all subjects, in 99% of the voxels $\lambda_2/\lambda_1 \approx 0.8$. MEG signal power therefore is mostly contained in the first two principal components, as expected following the well-established theory regarding MEG quasi-silent pseudo-radial generators (Hämäläinen et al., 1993). Since the third component is very small, its retention in MIM estimation (Eq. (7)) introduces an indeterminate form, which is numerically unstable. Therefore, only the first two components, namely, λ_1, λ_2 and $[\hat{q}_{j\lambda 1}(t)\ \hat{q}_{j\lambda 2}(t)]$, where used to estimate seed-based MEG functional connectivity in terms of the Multivariate Interaction Measure.

3. Complex valued coherence

The Multivariate Interaction Measure (MIM) is based on complex valued coherence. Given two time domain signals, $x_k(t)$ and $x_l(t)$, and their Fourier transforms, $X_k(f)$ and $X_l(f)$, coherence is defined as

$$\mathrm{Coh}_{kl}(f) \equiv \frac{C_{kl}(f)}{\sqrt{C_{kk}(f)C_{ll}(f)}}, \quad (2)$$

where

$$C_{kl}(f) \equiv \langle X_k(f)X_l^*(f)\rangle \quad (3)$$

is the cross spectrum between $X_k(f)$ and $X_l(f)$, $C_{kk}(f)$ is the power spectrum of $X_k(f)$, and $C_{ll}(f)$ is the power spectrum of $X_l(f)$. The symbols * and $\langle\ \rangle$ in Eq. (3) indicate complex conjugation and expectation value, respectively. In practice, the expectation value is estimated as the average over signal epochs. In the following, frequency dependence of all the quantities is implicitly understood. Complex valued coherence in Eq. (2) can be split into

its real and imaginary part, the former being sensitive to in-phase and phase-shifted interactions and the latter being non vanishing only for phase-shifted interactions. Expressing X_k and X_l in phasor notation explicitly shows their dependence on amplitude (a_k and a_l respectively) and phase (Φ_k and Φ_l respectively)

$$X_k = a_k e^{J\Phi_k} = a_k(\cos\Phi_k + J\sin\Phi_k)\ X_l = a_l e^{J\Phi_l} = a_l(\cos\Phi_l + J\sin\Phi_l), \quad (4)$$

where J stands for the imaginary unit. It immediately follows that C_{kl} can be expressed as

$$C_{kl} = \left\langle a_k e^{J\Phi_k} (a_l e^{J\Phi_l})^* \right\rangle = \left\langle a_k a_l e^{J(\Phi_k - \Phi_l)} \right\rangle = \left\langle a_k a_l e^{J\Delta\Phi} \right\rangle \quad (5)$$

A non- vanishing imaginary part of complex valued coherence can only result from a consistently phase-shifted relation between X_k and X_l. As a consequence of these properties, and assuming the quasi static regime for Maxwell's equations (instantaneous signal propagation of brain currents to MEG sensors), the imaginary component of Coh_{kl} is robust (in the above defined sense) to spurious connectivity caused by linear signal leakage between source space current estimates at spatially separate locations in the brain (Schoffelen & Gross, 2009; Sekihara et al., 2011) and to cross talk at the sensor level (Nolte et al., 2004). A significant deviation from zero of the imaginary component of complex valued coherence cannot be generated by independent sources, only by true interaction. Thus, the imaginary component of complex valued coherence robustly measures functional connectivity (Guggisberg et al., 2008; Martino et al., 2011; Marzetti et al., 2008; Nolte et al., 2009).

4. Connectivity map estimation by MIM

As outlined above, the estimated signal at each voxel, $[\hat{q}_{j\lambda 1}(t)\ \hat{q}_{j\lambda 2}(t)]$, is bi-dimensional. Therefore, to map global functional connectivity between voxel pairs, a pairwise interaction measure such as the imaginary part of coherence as defined above is not adequate. Rather, a measure of interaction between multidimensional subspaces is needed. For this purpose, we use the Multivariate Interaction Measure recently introduced by Ewald et al. (2012). Let us define $[\hat{q}_{s\lambda' 1}(t)\ \hat{q}_{s\lambda' 2}(t)]$ as the time domain signals at the seed voxel s, and $[\hat{q}_{j\lambda 1}(t)\ \hat{q}_{j\lambda 2}(t)]$ as the time domain signals at a generic voxel j (Figure 1).

The Fourier transform of these signals can be expressed as the vectors $X_s(f) = [\hat{Q}_{s\lambda' 1}(f)\ \hat{Q}_{s\lambda' 2}(f)]$ and $X_j(f) = [\hat{Q}_{j\lambda 1}(f)\ \hat{Q}_{j\lambda 2}(f)]$, spanning two bi-dimensional subspaces. Further introducing the notation $X(f) = [X_S^T(f) X_j^T(f)]^T$, the cross-spectrum between the two vectors assumes the block form:

$$C(f) = \langle X(f) X(f)^* \rangle = \begin{pmatrix} C_{ss}^R(f) + JC_{ss}^I(f) & C_{sj}^R(f) + JC_{sj}^I(f) \\ C_{js}^R(f) + JC_{js}^I(f) & C_{jj}^R(f) + JC_{jj}^I(f) \end{pmatrix}, \quad (6)$$

where the superscripts R and I denote the real and the imaginary part, respectively. Complex coherence between the two subspaces is defined, analogously to the bivariate case, as the cross-spectrum normalized by power. We are interested in the imaginary part of the global complex coherence and, in particular, in finding the vector weights ($\alpha \in \Re^{2\times 1}$ and $\alpha \in \Re^{2\times 1}$) for the corresponding voxel directions that maximize the imaginary part of coherence between the two projections within subspaces of the seed voxel s and the generic voxel j. This idea is related to canonical correlation analysis (CCA) (Hotelling, 1936), which maximizes the correlation between multivariate data sets.

The maximum imaginary coherence between the two projections within the subspaces is found by setting to zero the derivatives of the imaginary part of coherency between the two virtual channels given by the weighted dipole directions with respect to the weights α and β (see Ewald et al., 2012 for details). This is equivalent to solving a set of eigenvalue equations. Each solution (eigenvalue) might be considered as a meaningful measure of brain interaction. Nevertheless, to derive a global index for coupling between multidimensional voxel signals, we sum the eigenvalues in quadrature (compute the square root of the sum of all eigenvalues squared), i.e., MIM. An alternative definition of MIM can be analytically derived without directly solving the set of eigenvalue equations (see again Ewald et al., 2012 for analytical derivation), thus providing the compact form:

$$\mathrm{MIM_{sj}}=tr\left(\left(C_{ss}^{R}\right)^{-1}C_{sj}^{I}\left(C_{jj}^{R}\right)^{-1}\left(C_{sj}^{I}\right)^{T}\right), \quad (7)$$

where, for notational simplicity, the dependence on the frequency is again omitted. Thus, the MIM analytical formulation finds the dipole orientations that maximize the imaginary coherence for a given pair of sources. This is equivalent to performing an exhaustive search over each orientation in the dipole subspaces and estimating the imaginary coherence for each orientation pair. We emphasize that MIM is invariant to linear and static transformations within the subspace spanned by each vector signal, but not to the coupling between two subspaces. If a measure not invariant to linear transformations of the 3D coordinates for a given voxel were used, such as the averaged imaginary coherence between different possible orientations, the interaction result would depend on the orientation of the coordinate system and would therefore be meaningless. As was shown in Ewald et. al. (2012), an interaction measure for which the invariance properties holds must have the form given in Eq. (7).

In this work, MIM values were estimated as follows: Cross-spectra were averaged over approximately 400 signal epochs of 1.5 s duration with 50% overlap between epochs (frequency resolution of 0.66 Hz), after linear de-trending and Hanning windowing. To further improve the interaction estimate robustness, consecutive frequency bins were integrated over frequency bands defined on the basis of individual alpha peak (IAF) (Klimesch, 1996). In our data, IAF variability was 10.1±0.7 Hz (mean ± standard deviation). The alpha band was defined for each subject as IAF±2Hz; the definitions of other frequency bands were individually adjusted accordingly. On average, these bands span the following frequency ranges: delta (2–3.5 Hz), theta (4–7 Hz), alpha (8–12 Hz), beta (13–30 Hz), in accordance with conventional practice (Engel & Fries, 2010). Results for frequencies above 30 Hz (gamma band range) did not reveal significant interactions and therefore are not reported here.

Since MIM is a positive definite quantity, cross-spectral estimates in Eq. (7) based on a finite number of epochs will be positively biased. This bias can be approximated by assuming that the original signal is a superposition of independent sources over K trials and that mixing artifacts exist within but not across subspaces. Thus, an approximated expectation value for the MIM bias is given by

$$\langle \mathrm{MIM_{sj}} \rangle \approx \frac{N_s N_j}{2K} \quad (8)$$

where $\langle \cdot \rangle$ denotes expectation value, N_s and N_j are the subspace dimensions and K is the number of trials used for cross-spectral estimation. In this work, we computed the empirical distribution of MIM for independent sources (simulated as i.i.d. Gaussian noise) using a Monte Carlo approach, the mean of which corresponds to Eq. (8). A non-parametric

Wilcoxon signed-rank test was used to assess voxel-wise significance of MIM maps across subjects. For each frequency band and seed, the MIM distribution across subjects for each voxel was compared to the empirical distribution of MIM for independent sources. Significant voxels were assessed with Bonferroni correction for multiple comparisons across voxels ($p<0.001$, corrected value). Significant voxels then were included in a binary group mask. Specifically, the steps of the group statistics for a given frequency band were as follows: i) for each seed, the MIM distribution across subjects for each voxel is the input to the Wilcoxon signed rank test. Voxels significantly different from the empirical distribution for i.i.d. noise were assigned a value of 1, and all other voxels were set to 0 to generate a binary mask; ii) a binary valued conjunction mask was obtained by combining the single seed binary masks by a logical AND; iii) for each seed, the group average MIM was computed; iv) the mean group MIM map across the two seeds was computed; v) the final map is obtained by masking the average obtained in iv) with the conjunction mask derived in ii).

MIM mapping was applied to derive functional connectivity maps between nodes in the dorsal attention network (DAN) and voxels in the whole brain space. The principal nodes of the DAN bilaterally include anterior and posterior intraparietal sulcus (IPS), the intersection of precentral and superior frontal sulcus (human FEF), and the middle temporal area (MT). Posterior IPS (pIPS) and human FEF in the left hemisphere were selected as seeds for functional connectivity mapping. These nodes have been defined based on a meta-analysis of fMRI studies of spatial attention described in He et al. (2007); their coordinates in Montreal Neurological Institute (MNI) space are listed in the first two rows of Table 1 (see also de Pasquale et al., 2010). Final pIPS-FEF conjunction maps were obtained as described above. All maps were projected to the brain surface for visualization by using Caret software (http://www.nitrc.org/projects/caret/, Van Essen et al., 2001).

5. Frequency specificity of MIM values

ANOVA was used to statistically assess frequency specificity within and between network interactions. Since MIM values for background brain activity differ across frequency bands, we normalized for global MIM values by calculating *Normalized MIM*. This quantity is obtained by correcting MIM by its mean and standard deviation (Z-score) over the whole brain in each subject and for each frequency band. Specifically, the normalization was performed on the conjunction map of lFEF and lPIPS seeds. Thus, all ANOVA tests were run using the *Normalized MIM*. Two-way ANOVA were run on *Normalized MIM* values with Band (delta, theta, alpha, beta) and Network Node as factors. The Network Node can either be DAN nodes or nodes belonging to the other RSNs that showed interactions with DAN nodes. In addition, if one frequency band was found to be involved in within and between interactions, a one-way ANOVA with factor Network was performed to evaluate possible differences related to phase-lag of within versus between network interactions.

RESULTS

1. Multivariate Interaction Map within the dorsal attention network

The group MIM map obtained for the left hemisphere FEF (lFEF) seed is shown in Figure 2 for the alpha frequency band.

The seed position is indicated by a blue dot. The group MIM map shows interactions both within the seeded hemisphere and inter-hemispherically. In particular, if we focus on DAN regions, we observe that nodes of the right hemisphere (i.e. rFEF, rpIPS) show out of phase coherent interactions. The other topographies obtained by seeding either the lFEF or the

lPIPS for the delta, alpha and beta frequency bands prior to the conservative conjunction procedure are shown in the Supplementary Material (Figure S1).

Figure 3 (a, b) shows the generalization of MIM mapping across the two core regions of the DAN (pIPS, FEF) obtained as the conjunction map for the delta and alpha frequency bands. Conjunction maps are necessarily more sparse than the union of the individual maps. Two effects stand out from this conjunction map. First, nonzero phase coupling between seeds in the left hemisphere and the rest of the brain is predominantly contralateral, and this coupling exhibits substantial topographic specificity, that is, is greatest in the right hemisphere near nodes of the DAN. Second, there is substantial frequency specificity, as shown in Figure 3c for the inter-hemispheric MIM [both nodes (rFEF and rpIPS)].

To statistically assess this frequency specificity, we ran a 2-way ANOVA on *Normalized MIM* values (see Methods section) with Band (delta, theta, alpha, beta) and DAN Node (rpIPS, rFEF) as factors. This ANOVA returned a significant main effect of Band ($F(3,69)=2.6$, $p<0.05$). As shown in Figure 3d, statistically significant differences were detected between alpha and theta and alpha and beta as well as between delta and theta and delta and beta ($p<0.05$). There was no significant difference between alpha and delta, which is consistent with the topographic similarity of the two maps shown in Figure 3 (a, b).

2. Multivariate Interaction Measure between networks

Our analysis also detected phase-shifted functional connectivity between different networks. Specifically, significant MIM was observed in the alpha band between DAN nodes and visual areas (see Table 1 for node coordinates). The topography of this interaction is shown in Figure 4a, which shows the posterior view of Figure 3b, i.e., the conjunction map obtained from the left FEF and left pIPS group maps in the alpha band. This figure illustrates temporally delayed interactions of left hemisphere nodes of the DAN with bilateral lower and higher order visual areas.

A 2-way ANOVA on individual *Normalized MIM* values obtained from visual network nodes (lV1, lV2v, lV3, lV4, rV1v, rV2d, rV3) was run with factors Band and Node. This analysis showed a main effect of Band ($F(3,69)=5.75$, $p=0.0014$). Post-hoc tests confirmed that non-zero-phase interaction between DAN nodes and visual network nodes were significantly stronger in alpha than in theta and beta ($p<0.003$). Only a trend was observed in the delta band, which suggests that the alpha band is particularly important in mediating interactions between the DAN and visual areas (Fig. 4b). In addition, confining the analysis in the alpha band, a one-way ANOVA with factor Network (averaging regions from DAN in the contralateral hemisphere (rpIPS, rFEF) and bilateral visual network nodes (lV1, lV2v, lV3, lV4, rV1v, rV2d, rV3) respectively) was run to evaluate possible differences related to phase-lag of DAN-Visual network interaction with respect to within-DAN interaction. ANOVA results ($F(1,23)=5.03$, $p<0.04$) revealed that *Normalized MIM* between the DAN and visual nodes is greater than between homologous nodes within the DAN (Figure 4c).

Evidence for between network interactions as mapped by MIM was also found between the DAN and the somatomotor network. Interestingly, this coupling was found in the beta frequency range. Figure 5a shows the corresponding topography obtained from the conjunction map of the left FEF and pIPS group maps in the beta band. This map provides evidence for phase-shifted DAN interactions with primary and secondary somatomotor cortex both in left and in right hemispheres.

A 2-way ANOVA of individual *Normalized MIM* values obtained from the somatomotor network nodes (lCS, lS2, lPMA, rS2, SMA) was run with factors Band and Node. This analysis showed a main effect of Band ($F(3,69)=3.3$, $p<0.03$). Post-hoc tests confirmed that

non-zero-phase interaction between DAN nodes and these somatomotor network nodes were significantly stronger in beta than in all the other frequency bands ($p<0.01$, beta vs. delta and beta vs. alpha; $p=0.05$, beta vs. theta), see Figure 5b.

A one-way ANOVA with factor Network was run confining the analysis to the beta band. In this analysis, DAN regions in the contralateral hemisphere (rpIPS, rFEF) and bilateral somatomotor network (lCs, lS2, rCS, rS2, SMA) were collapsed with the aim of evaluating possible differences related to phase-lag of DAN-Somatomotor network interaction with respect to within-DAN interaction. ANOVA results ($F(1,20)=8.64$, $p<0.008$) are shown in Figure 5c and reveal that *Normalized MIM* values within the somatomotor network nodes are significantly higher than those within the DAN. To further investigate this effect, we run another one way ANOVA in which nodes within each network were not collapsed. ANOVA results ($F(6,138)=2.57$, $p =0.02$) are shown in Figure 5d and reveal that, also for single nodes, *Normalized MIM* values for the somatomotor network nodes are significantly higher than values for DAN nodes.

DISCUSSION

We examined phase-shifted coherence of resting-state neuromagnetic signals within and between functional networks previously defined by fMRI. This work, as far as we are aware, represents the first report of phase-shifted, source-space neuromagnetic interactions linked to fMRI-derived networks. Non zero-phase interactions were observed between homologous left and right hemisphere regions of the DAN in the delta and alpha frequency bands. Furthermore, even stronger non zero-phase interactions were detected between networks. Visual regions bilaterally showed interactions in the alpha band with regions of the DAN; bilateral somatomotor regions interacted with DAN nodes in the beta band.

1. MEG vs. fMRI functional connectivity

The observation that MEG MIM topography resembles RSNs derived by fMRI is remarkable because the two modalities operate in non-overlapping temporal frequency bands (~0.01 – 0.1 Hz in the case of fMRI vs. 1–100 Hz in the case of MEG). Also, it should be noted that resting state fMRI correlations, with rare exceptions, e.g., (Roebroek et al., 2011), are computed at zero phase lag. Non-zero phase lags in resting state fMRI data are widely assumed to be un-interpretable because blood oxygenation level dependent (BOLD) signals only indirectly reflect neural activity and the kinetics of the hemodynamic transduction mechanism cannot be directly observed (Smith et al., 2012). The two modalities also operate in non-overlapping spatial frequency bands: the spatial resolution of MEG is limited by the intrinsic nature of the electromagnetic inverse problem, while the spatial resolution of fMRI is limited only by practical considerations governing the achievable magnetic field and imaging gradient strengths (I mm resolution throughout the brain is feasible at 7 tesla, Ugurbil K, 2012). Moreover, whereas MEG is relatively insensitive to sources distant from the sensors, e.g., the mesial and inferior cortical surfaces, fMRI coverage is not similarly limited. Nevertheless, there exists an obvious topographic concordance between the present results and the extant resting state fMRI literature (e.g., compare present Figure 3 to Figure 5 of Fox et al., 2006).

If the upper frequency limit of physiologically meaningful signals in an MEG record is conservatively taken to be 30 Hz, we can estimate the number of independent measures (per channel) in a 5-minute record as $2 \cdot 5 \cdot 60 \cdot 30 = 18{,}000$. In contrast, if the upper frequency limit of physiologically meaningful fMRI signals is taken to be 0.1 Hz (Hathout et al., 1999), there are only 60 independent measures (per voxel) in a 5-minute record. This difference in spectral content translates to a substantial difference in information acquired over a typical resting state epoch. Thus, MEG supports a wide variety of analytic strategies for

characterizing signal interactions between ROI pairs that are not accessible to fMRI. MIM is only one such strategy. Alternative strategies include correlation of band-limited power in the 3–30 Hz range (Brookes et al., 2011a; Brookes et al., 2011b; de Pasquale et al., 2010; de Pasquale et al., 2012) and several techniques for estimating directed influences between ROI pairs as reviewed in (Castellanos et al., 2011; Florin et al., 2011; Schnitzler & Gross 2005; Schoffelen & Gross 2008).

2. Multivariate Interaction Measure in resting state MEG

Phase-shifted interactions were derived from the Multivariate Interaction Measure (MIM), a quantity based on maximizing the imaginary part of coherence between multidimensional subspaces (Ewald et al., 2012; Nolte et al., 2004). Low spatial resolution of MEG source space projection introduces artificial zero-lag coherence, usually defined as the field spread effect (Brookes et al., 2012; Hauk et al., 2011; Schoffelen & Gross, 2009). State contrast, e.g., control vs. task periods, has been used to null-out zero-phase interactions under the assumption that they are identical in both conditions. This strategy cannot be applied to resting state data because task contrast does not exist. The imaginary part of coherence is known to systematically ignore any functional relation occurring at vanishing phase delay, including artifacts from volume conduction in channel space and of field spread in source space, and can therefore provide information about true non zero-lag interactions even in the absence of task contrast.

Functional connectivity based on the imaginary part of coherence reflects a consistent out-of-phase relationship that generally depends on both power and phase. In noisy data, this combination of effects persists, even if we study only phase relations at estimated sources, e.g., by phase locking value (Varela et al., 2001), because the observed phase depends not only on the true signal phase but also on signal to noise ratio within each trial. In fact, an amplitude decrease of the coherent process of interest, say without any change in phase difference, will result in an overall increased phase difference in the presence of a highly correlated background noise. On the other hand, a measure of interaction based on amplitude-weighted phase, such as the imaginary part of coherence, theoretically provides a statistically more robust estimator of phase relationships for weak signals (Nolte et al., 2004).

3. Comparison between the Multivariate Interaction Measure and the scalar approach

The imaginary part of coherence is a bivariate measure of interaction between uni-dimensional signals. When dealing with MEG source space signals, uncertainty in functional to anatomical image coregistration prevents the use of a strict cortical orientation constraint to fix dipole direction (Chang et al., 2012). Therefore, the estimated signal at each location must be treated as a vector in a multidimensional subspace. To investigate the question of coherence/phase synchrony, it is necessary to extend the classical definitions (Nolte et al., 2004; Varela et al., 2001) to pairs of multivariate time series. The MIM measure provides an extension such that invariance to the orientation of the coordinate system is achieved. Such extension is needed also when connectivity is mapped from source space signal estimated by vector beamformers (Sekihara et al., 2001) in which the three components of the weight vector are used to track the three components of the source activity. The MIM method is based on the maximization of the imaginary part of coherence between the seed and the test voxel vector activity thus leading to an increase in signal to noise ratio by construction potentially allowing to observe interactions otherwise embedded into noise. This feature is particularly relevant for low amplitude resting state signals. An alternative approach is the selection of the direction of maximum power, e.g. using PCA to determine a fixed dipole direction (Sekihara et al., 2004), thus mapping connectivity between scalar quantities (e.g., by standard Imaginary coherence). However, the directions of maximal power can in general

be quite different from the directions which maximize imaginary coherence. With the power based approach, we might miss local interactions as well as interactions which correspond to weak sources, i.e. the stronger sources are not always the interacting ones. To investigate this, we made illustrative calculations from MEG data measured in a single subject under resting condition for 20 minutes. At sensor level, we observed a strong peak of imaginary coherence (ImCoh) at 20.5 Hz which was analyzed by projecting crossspectra at the source level using a weighted minimum norm source reconstruction. For two voxels, we calculated source activities for all source directions in the two-dimensional plane spanned by the two eigenvectors corresponding to the two largest eigenvalues of the real part of the cross-spectrum at 20.5Hz. Since we have two voxels, we have two of such directions defined by Φ_1 and Φ_2. We calculated the imaginary part of coherence and the sum of powers of the two dipoles for all pairs of angles, each in the range $[0, \pi]$. We consider two situations: i) the two voxels are far apart and located one in the left and one in the right motor area (Figure 6, panels a and b); ii) the two voxels are identical and located in the left motor area (Figure 6, panels c and d).

From the above figure, we first observe that the sum of powers is always maximal at the corners (b, d) which are physically equivalent and just differ by the sign of the activity. This is consequence of the chosen basis: vanishing angles correspond to the direction of eigenvector with largest eigenvalue, i.e. largest power. One of these corners would be chosen if the direction of the dipoles would be fixed corresponding to maximal power. For ImCoh, we observe that maximal values do not correspond to the corners. Specifically, for identical voxels ImCoh vanishes exactly on the diagonal (c) (and in all corners) because this corresponds to self-interaction which cannot be detected by ImCoh. In the MIM approach we can observe an interaction with itself because it includes non-identical orientations which pick up signals from different sources. For remote interactions, ImCoh is almost vanishing in our example (a). We consider this as a coincidence which is not necessarily the case but shows that it is possible that interactions are missed if dipole directions are fixed according to power.

To further show the difference between the MIM approach and the scalar approach based on estimating the imaginary part of coherence between the first principal direction at the seed and at all other voxels, we provide a representative example of such comparison in the alpha band. Figure 7 (a) shows the MIM map for the lFEF seed (also shown in figure 2) and the corresponding scalar map (b). In the scalar version, we map the squared imaginary coherence which is dimensionally consistent with MIM values (Ewald et al., 2012). This comparison shows that although the two topographies share some commonalities, they also present clear differences. In particular, the right pIPS is highlighted by both approach but the rFEF is present only in the MIM map. On the other hand, other right frontal regions are significant in the scalar map but lose their significance when the vector measure is taken into account. Moreover, overall increased values are found for the MIM map meaning that an important part of the interaction could be lost with the scalar approach.

In conclusion, by taking only orientation of maximum power and ignoring the orthogonal direction, we miss local interactions. Minimum norm inverse solutions, like beamformer solutions, are spatially very blurred. If there are two interacting sources close to each other, say e.g. at 4mm distance, then these inverse methods will mix the activities. For simplicity of the argument let's assume that the sources are located exactly on two neighboring voxels but have different orientations. The estimates of the source activities at these two voxels will contain activity of both sources, such that, as the most likely result, the dipole direction of both voxels will correspond to the one of the stronger source. The interaction is then not visible or perhaps will reappear as long range interaction in a weaker form. Thus, in general we would have a bias towards remote interactions. The second kind of interactions possibly

missed are those corresponding to weak sources, as it is conceivable that the strong sources are not the interacting ones.

4. Putative neurobiological mechanisms

Non zero-phase coupling was observed between homologous nodes of the DAN (pIPS, FEF), within-network interaction, but was even higher for between network interactions, e.g., between DAN and visual regions, or DAN and regions of the somatomotor networks (Figs. 4 and 5). This finding suggests that between- as opposed to within-network interactions are relatively delayed, possibly because signals are routed through more complicated sub-cortical pathways. Inter-hemispheric as compared to intra-hemispheric interactions also appear relatively more delayed. Phase-shifted interactions fundamentally imply two mechanisms: synaptic delays between regions, and multi-synaptic pathways. Three main anatomical systems support information processing between cortical regions: intra-hemispheric association pathways; callosal pathways; and, cortico-striatal-thalamic-cortical loops.

We propose that inter-hemispheric phase-shifted interactions depend on the corpus callosum. The available evidence, albeit scarce, suggests that inter-hemispheric callosal connections are fewer, more variable in size and in degree of myelination, and contain a higher proportion of non-myelinated slow conducting fibers than intra-hemispheric cortical association pathways (Novack & Bullier, 1997). Evolutionary studies indicate that callosal connections increase in size as well as in size variability proceeding from macaques to chimpanzees to humans (Caminiti et al., 2009). Furthermore, the largest myelinated axons and the smallest proportion of unmyelinated axons (≈ 6%) are found in regions of the corpus callosum that carry projections from primary sensory cortices, whereas the smallest myelinated axons and largest proportion of un-myelinated axons (≈ 30%) are found in regions of the corpus callosum that carry projections from association cortices (prefrontal, parietal) (LaMantia & Rakic, 1994). As pointed out by Caminiti and colleagues (2009) slowing conduction and increasing the range of delays might expand the temporal domain for differentiation neuronal spike timing, enlarge the number of neuronal groups that cortical connectivity can generate, and facilitate oscillations through the interplay of inhibitory and excitatory conduction delays between the hemispheres (Caminiti et al., 2009). Our findings confirm the presence of lagged interaction between homologous regions of the prefrontal and parietal human cortex in the awake resting state.

5. Frequency specificity of MIM

We present evidence for frequency specificity in delta, alpha and beta phase-shifted interactions within and between RSNs. The temporal frequencies at which MIM is observed, i.e., ~ 3–30 Hz, agree with results obtained by invasive recording in monkeys (Wang et al., 2012). A possible theoretical basis for such results can be found in recent computational studies indicating that phase-shifted synchronization may be an important mechanism to link fast to slow RSN dynamics. In fact, when brain regions are modeled as biologically plausible coupled oscillators operating at high frequencies (e.g., in the gamma band), and connected by a veridical neuroanatomical matrix, then slow power fluctuations emerge when conduction delays between regions are introduced in the model (Cabral et al 2011; Deco et al., 2009; Ghosh et al., 2008). The relationship between slow fluctuation fMRI RSNs and activity/power and synchrony/coherence in electrophysiological data currently is an active field of investigation in real data. Prior studies have evaluated MEG data in terms of band-limited power (BLP), that is, the envelope of rhythmical activity at faster frequencies (nominally, 1–100 Hz) (Brookes et al., 2011a; Brookes et al., 2011b; de Pasquale et al., 2010; de Pasquale et al., 2012; Liu et al., 2010). Weak links between MEG BLP and imaginary part of coherence have also been recently presented (Brookes et al.,

2010). Correlations of slow frequency (nominally, below 0.1 Hz) power fluctuations as measured by MEG generate RSN topographies similar to those observed by fMRI. Our previous papers (de Pasquale, 2010 & 2012) suggest that low frequency BLP correlations exhibit fMRI RSN topographies only transiently, and non-stationarity must be explicitly taken into account to demonstrate MEG-fMRI correspondences. Here, we demonstrate that phase-shifted interactions between nodes of networks or between networks seem to be robust over relatively long time periods (minutes), although it is likely that transient modulations of phase relationships, strong enough to show up after averaging over time, occur over shorter time scales.

The spectral specificity of our presently observed MIM results may also have systems-level neurobiological implications. One important observation is that MIM between RSNs at rest involves similar frequencies to those observed during tasks. Homologous regions of the DAN (pIPS, FEF) maintain phase-shifted interactions in the alpha band (and, to a lesser extent, the delta band). DAN and visual cortex maintain phase-shifted interactions in the alpha band while DAN and somatomotor cortex maintain phase-shifted coupling in the beta band. The DAN has been described as a control network for directing spatial attention to sensory representations and linking relevant sensory-to-motor representations (Corbetta and Shulman, 2002; Culham & Kanwisher, 2001; Rushworth et al., 2001). The relationship between DAN and alpha rhythms is consistent with previous EEG/MEG work showing an association with alpha power envelope fluctuations (de Pasquale et al., 2010 & 2012; Laufs et al., 2003; Mantini et al., 2007). Alpha power also is consistently modulated in electroencephalographic (EEG) studies of attention and visuo-motor tasks (Capotosto et al., 2009; Worden et al., 2000; Thut et al., 2006) that also strongly recruit the DAN (Corbetta and Shulman, 2002; Culham & Kanwisher, 2001; Rushworth et al., 2001).

An emerging literature indicates that communication between control systems and data processing systems may involve different frequencies (Engel and Fries, 2010; Fries et al., 2005). Directing spatial attention to a visual field location modulates occipital cortex alpha power, possibly reflecting an active suppression of unattended locations (Foxe et al.,1998; Kelly et al.,2006; Worden et al.,2000; Snyder & Foxe, 2010; Thut et al.,2006). Direct causal evidence of interaction comes from transcranial magnetic stimulation (TMS) studies. Disruption of FEF or pIPS anticipatory activity during a spatial attention task alters the normal modulation of alpha-band activity over occipital visual cortex, and impairs behavioral performance (Capotosto et al., 2009; Capotosto et al 2010; Romei et al., 2010). Hence interactions in the alpha band seem to occur between visual occipital and frontoparietal cortex both at rest and during visuomotor attention tasks.

Similarly, beta rhythms have been associated with somatomotor activity at rest, and index frequency-specific interactions between DAN and sensory-motor cortex during attention tasks (Anderson & Ding, 2011; Haegens et al., 2011; Johansen-Berg & Matthews, 2002; Jones et al., 2010; Rushworth et al., 2001; van Ede et al., 2011). In particular, orienting to an anticipated tactile event induces pre-stimulus suppression of sensori-motor alpha and beta band oscillations contralateral to the attended side (Van Ede et al., 2011) similarly to what observed in the visual cortex with alpha rhythms (Foxe et al.,1998; Kelly et al.,2006; Worden et al.,2000; Thut et al.,2006). Finally, modulations of beta synchronization have been reported with visual fixation, eye movements and shifts of attention in FEF (Buschmann & Miller, 2007; Drewes & VanRullen, 2011).

6. Future directions

The present work represents the first report of source-space phase-shifted interactions robust over relatively long time periods (minutes) in RSNs as derived from fMRI. Our results demonstrate the effectiveness of the MIM measure in resting state MEG and are sufficient to

distinguish within- vs. across- network lagged phase relations for DAN. It is likely that these relations will generalize to other networks, as an all-to-all mapping approach might reveal (Palva et al., 2012). Moreover, the use of a multidimensional measure opens the way for characterizing interactions between higher dimensional subspaces, e.g. those defined from cortical patches on the basis of cytoarchitectonics or functional organization.

Other possible strategies for assessing lagged phase interactions, such as the lagged coherence defined in (Pascual-Marqui, 2007; Pascal-Marqui et al., 2011), the Phase Lag Index (Hillebrand et al., 2012; Stam et al.,2007) and the Weighted Phase Lag Index (Vinck et al., 2011) may reveal different RSN features. Indeed, a multivariate framework has been used by Brookes and colleagues (2012) to address the problem of signal leakage by regressing out the zero-phase lag component of the seed signal over the whole frequency span by the source signal at all other brain voxels. The method has been applied successfully to investigate power-to-power coupling within the motor network. The use of such approach for MEG signal would result in a strategy closely related to the MIM approach. Measures based on higher order frequency domain statistical moments and robust to mixing distortions could be very powerful tools for investigating cross frequency coupling in RSNs (Jensen & Colgin, 2007; Palva et al., 2005; Palva et al., 2012). We look forward to comparisons of these methods.

Supplementary Material

Refer to Web version on PubMed Central for supplementary material.

Acknowledgments

This work was supported by the European Community's Seventh Framework Programme (FP7/2007–2013), Grant Agreement n HEALTH-F2-2008-200728 'BrainSynch', NIH grant MH 71920- 06, and the Human Connectome Project (1U54MH091657-01) from the 16 National Institutes of Health Institutes and Centers that support the NIH Blueprint for Neuroscience Research.

REFERENCES

1. Anderson KL, Ding M. Attentional modulation of the somatosensory mu rhythm. Neuroscience. 2011; 180:165–180. [PubMed: 21310216]
2. Biswal B, Yetkin FZ, Haughton VM, Hyde JS. Functional connectivity in the motor cortex of resting human brain using echo-planar MRI. Magn Reson Med. 1995; 34:537–541. [PubMed: 8524021]
3. Brookes MJ, Hale JR, Zumer JM, Stevenson CM, Francis ST, Barnes GR, Owen JP, Morris PG, Nagarajan SS. Measuring functional connectivity using MEG: Methodology and comparison with fcMRI. NeuroImage. 2011a; 56:1082–1104. [PubMed: 21352925]
4. Brookes MJ, Woolrich M, Luckhoo H, Price D, Hale JR, Stephenson MC, Barnes GR, Smith SM, Morris PG. Investigating the electrophysiological basis of resting state networks using magnetoencephalography. Proc Natl Acad Sci U S A. 2011b; 108:16783–16788. [PubMed: 21930901]
5. Brookes MJ, Woolrich M, Barnes GR. Measuring functional connectivity in MEG: A multivariate approach insensitive to linear source leakage. Neuroimage. 2012; 63:910–920. [PubMed: 22484306]
6. Buckner RL, Krienen FM, Castellanos A, Diaz JC, Yeo BT. The Organization of the Human Cerebellum Estimated By Intrinsic Functional Connectivity. J Neurophysiol. 2011; 106:2322–2345. [PubMed: 21795627]
7. Cabral J, Hugues E, Sporns O, Deco G. Role of local network oscillations in resting-state functional connectivity. NeuroImage. 2011; 57:130–139. [PubMed: 21511044]

8. Caminiti R, Ghaziri H, Galuske R, Hof PR, Innocenti GM. Evolution amplified processing with temporally-dispersed, slow, neural connectivity in primates. Proc Natl Acad Sci USA. 2009; 106:19551–19556. [PubMed: 19875694]
9. Capotosto P, Babiloni C, Romani GL, Corbetta M. Frontoparietal cortex controls spatial attention through modulation of anticipatory alpha rhythms. J Neurosci. 2009; 29:5863–5872. [PubMed: 19420253]
10. Capotosto P, Babiloni C, Romani GL, Corbetta M. Differential Contribution of Right and Left Parietal Cortex to the Control of Spatial Attention: A Simultaneous EEG–rTMS Study. Cerebral Cortex. 2010; 22:446–454. [PubMed: 21666126]
11. Castellanos NP, Bajo R, Cuesta P, Villacorta-Atienza JA, Paul N, Garcia-Prieto J, Del-Pozo F, Maestu F. Alteration and reorganization of functional networks: a new perspective in brain injury study. Frontiers in human neuroscience. 2011; 5:90. [PubMed: 21960965]
12. Chang W-T, Ahlfors SP, Lin F-S. Sparse Current Source Estimation for MEG Using Loose Orientation Constraints. Hum Brain Mapp. 2012
13. Cohen D. Magnetoencephalography: detection of the brain's electrical activity with a superconducting magnetometer. Science. 1972; 175(4022):664–666. [PubMed: 5009769]
14. Cole DM, Smith SM, Beckmann CF. Advances and pitfalls in the analysis and interpretation of resting-state FMRI data. Front Syst Neurosci. 2010; 4:8. [PubMed: 20407579]
15. Corbetta M, Shulman GL. Control of goal-directed and stimulus-driven attention in the brain. Nat Rev Neurosci. 2002; 3:201–215. [PubMed: 11994752]
16. Crick F, Koch C. A framework for consciousness, Nat. Neurosci. 2003; 6:119–126.
17. de Pasquale F, Della Penna S, Snyder AZ, Lewis C, Mantini D, Marzetti L, Belardinelli P, Ciancetta L, Pizzella V, Romani GL, Corbetta M. Temporal dynamics of spontaneous MEG activity in brain networks. Proc Natl Acad Sci U S A. 2010; 107:6040–6045. [PubMed: 20304792]
18. de Pasquale F, Della Penna S, Snyder AZ, Marzetti L, Pizzella V, Romani GL, Corbetta M. A cortical core for dynamic integration of functional networks in the resting human brain. Neuron. 2012; 74:753–764. [PubMed: 22632732]
19. Deco G, Jirsa V, McIntosh AR, Sporns O, Koetter R. Key role of coupling, delay and noise in the resting brain fluctuations. Proc Natl Acad Sci U S A. 2009; 106:10302–10307. [PubMed: 19497858]
20. Deco G, Corbetta M. The Dynamical Balance of the Brain at Rest. Neuroscientist. 2010; 17:107–123. [PubMed: 21196530]
21. Della Penna S, Del Gratta C, Granata C, Pasquarelli A, Pizzella V, Rossi R, Russo M, Torquati K, Erne SN. Biomagnetic systems for clinical use. Philos. Mag. 2000; 80:937–948.
22. Doucet G, Naveau M, Petit L, Delcroix N, Zago L, Crivello F, Jobard G, Tzourio-Mazoyer N, Mazoyer B, Mellet E, Joliot M. Brain activity at rest: a multiscale hierarchical functional organization. J Neurophysiol. 2011; 105:2753–2763. [PubMed: 21430278]
23. Drewes J, VanRullen R. This is the rhythm of your eyes: the phase of ongoing electroencephalogram oscillations modulates saccadic reaction time. J Neurosci. 2011; 31:4698–4708. [PubMed: 21430168]
24. Engel A, Fries P. Beta-band oscillations – signaling the status quo? Current Opinion in Neurobiology. 2010; 20:156–165. [PubMed: 20359884]
25. Ewald A, Marzetti L, Zappasodi F, Meinecke FC, Nolte G. Estimating true brain connectivity from EEG/MEG data invariant to linear and static transformations in sensor space. Neuroimage. 2012; 60:476–488. [PubMed: 22178298]
26. Florin E, Gross J, Pfeifer J, Fink GR, Timmermann L. Reliability of multivariate causality measures for neural data. Journal of neuroscience methods. 2011; 198:344–358. [PubMed: 21513733]
27. Fox MD, Snyder AZ, Vincent JL, Corbetta M, Van Essen D, Raichle ME. The human brain is intrinsically organized into dynamic, anticorrelated functional networks. Proc Natl Acad Sci USA. 2005; 102:9673–9678. [PubMed: 15976020]
28. Fox MD, Corbetta M, Snyder AZ, Vincent JL, Raichle ME. Spontaneous neuronal activity distinguishes human dorsal and ventral attention systems. Proceedings of the National Academy of Sciences of the United States of America. 2006; 103:10046–10051. [PubMed: 16788060]

29. Fox MD, Raichle ME. Spontaneous fluctuations in brain activity observed with functional magnetic resonance imaging. Nat Rev Neurosci. 2007; 8:700–711. [PubMed: 17704812]
30. Fries P. A mechanism for cognitive dynamics: neuronal communication through neuronal coherence. Trends Cogn Sci. 2005; 9:474–480. [PubMed: 16150631]
31. Fuchs M, Wagner M, Kohler T, Wischmann HA. Linear and nonlinear current density reconstructions. J. Clin. Neurophysiol. 1999; 16:267–295. [PubMed: 10426408]
32. Ghosh Y, Rho A, McIntosh R, Koetter R, Jirsa V. Cortical network dynamics with time delays reveals functional connectivity in the resting brain. Cognit Neurodyn. 2008; 2:115–120. [PubMed: 19003478]
33. Gross J, Schmitz F, Schnitzler I, Kessler K, Shapiro K, Schnitzler A. Anticipatory control of long range phase synchronization. Europ J Neurosci. 2006; 24:2057–2060.
34. Guggisberg AG, Honma SR, Findlay AM, Dalal SS, Kirsch HE, Berger MS, Nagarajan SS. Mapping functional connectivity in patients with brain lesions, Ann. Neurology. 2008; 63(2):193–203.
35. Haegens S, Haendel BF, Jensen O. Top-down control of alpha band activity in somatosensory areas determines behavioural performance in a discrimination task. J. Neurosci. 2011; 31:5197–5204. [PubMed: 21471354]
36. Hämäläinen M, Hari R, Ilmoniemi R, Knuutila J, Lounasmaa OV. Magnetoencephalography—theory, instrumentation, and applications to noninvasive studies of the working human brain. Rev. Mod. Phys. 1993; 65:413–497.
37. Hämäläinen M, Ilmoniemi R. Interpreting magnetic fields of the brain: Minimum norm estimates. Medical and Biological Engineering and Computing. 1994; 32:35–42. [PubMed: 8182960]
38. Hauk O, Wakeman DG, Henson R. Comparison of noise-normalized minimum norm estimates for MEG analysis using multiple resolution metrics. NeuroImage. 2011; 54:1966–1974. [PubMed: 20884360]
39. Hari R, Salmelin R. Magnetoencephalography: From SQUIDs to neuroscience. NeuroImage. 2012; 61:386–396. [PubMed: 22166794]
40. Hathout GM, Gopi RK, Bandettini P, Gambhir SS. The lag of cerebral hemodynamics with rapidly alternating periodic stimulation: modeling for functional MRI. Magnetic resonance imaging. 1999; 17:9–20. [PubMed: 9888394]
41. He BJ, Snyder AZ, Vincent JL, Epstein A, Shulman GL, Corbetta M. Breakdown of functional connectivity in frontoparietal networks underlies behavioral deficits in spatial neglect. Neuron. 2007; 53:905–918. [PubMed: 17359924]
42. Hillebrand A, Barnes GR, Bosboom JL, Berendse HW, Stam CJ. Frequency-dependent functional connectivity within resting-state networks: An atlas-based MEG beamformer solution. Neuroimage. 2012; 59:3909–3921. [PubMed: 22122866]
43. Hotelling H. Relations between two sets of variates. Biometrika. 1936; 28(3):321–377.
44. Jensen O, Colgin LL. Cross-frequency coupling between neuronal oscillations. Trends Cogn Sci. 2007; 11:267–269. [PubMed: 17548233]
45. Johansen-Berg H, Matthews PM. Attention to movement modulates activity in sensori-motor areas, including primary motor cortex. Exp. Brain Res. 2002; 142:13–24. [PubMed: 11797080]
46. Jones SR, Kerr CE, Wan Q, Pritchett DL, Hämäläinen M, Moore CI. Cued Spatial Attention Drives Functionally Relevant Modulation of the Mu Rhythm in Primary Somatosensory Cortex. J Neurosci. 2010; 30:13760–13766. [PubMed: 20943916]
47. Laird AR, Fox PM, Eickhoff SB, Turner JA, Ray KL, McKay DR, Glahn DC, Beckmann CF, Smith SM, Fox PT. Behavioral interpretations of intrinsic connectivity networks. Journal of cognitive neuroscience. 2011; 23:4022–4037. [PubMed: 21671731]
48. LaMantia AS, Rakic P. Axon overproduction and elimination in the anterior commissure of the developing rhesus monkey. J Comp Neurol. 1994; 340:328–336. [PubMed: 8188854]
49. Liu Z, Fukunaga M, de Zwart JA, Duyn JH. Large-scale spontaneous fluctuations and correlations in brain electrical activity observed with magnetoencephalography. Neuroimage. 2010; 51:102–111. [PubMed: 20123024]

50. Kelly SP, Lalor EC, Reilly RB, Foxe JJ. Increases in alpha oscillatory power reflect an active retinotopic mechanism for distracter suppression during sustained visuospatial attention. JNeurophysiol. 2006; 95:3844–3851. [PubMed: 16571739]
51. Klimesch W. EEG alpha and theta oscillations reflect cognitive and memory performance: a review and analysis. Brain Research Reviews. 1996; 29:169–195. [PubMed: 10209231]
52. Mantini D, Perrucci MG, Del Gratta C, Romani GL, Corbetta M. Electrophysiological signatures of resting state networks in the human brain. Proc Natl Acad Sci USA. 2007; 104:13170–13175. [PubMed: 17670949]
53. Mantini D, Della Penna S, Marzetti L, de Pasquale F, Pizzella V, Corbetta M, Romani GL. A signal processing pipeline for MEG resting state networks. Brain Connectivity. 2011; 1:49–59. [PubMed: 22432954]
54. Martino JM, Homna SM, Findlay AM, Guggisberg AG, Owen JP, Kirsch HE, Berger MS, Nagarajan SS. Resting Functional Connectivity in Patients with Brain Tumors in Eloquent Areas. Ann. Neurology. 2011; 69(3):521–532.
55. Marzetti L, Del Gratta C, Nolte G. Understanding brain connectivity from EEG data by identifying systems composed of interacting sources. NeuroImage. 2008; 42:87–98. [PubMed: 18539485]
56. Nolte G, Bai O, Wheaton L, Mari Z, Vorbach S, Hallet M. Identifying true brain interaction from EEG data using the imaginary part of coherency. Clin. Neurophysiol. 2004; 115:2292–2307. [PubMed: 15351371]
57. Nolte G, Marzetti L, Valdes Sosa P. Minimum Overlap Component Analysis (MOCA) of EEG/MEG data for more than two sources. J Neurosci Methods. 2009; 183:72–76. [PubMed: 19596027]
58. Palva JM, Palva S, Kaila K. Phase synchrony among neuronal oscillations in the human cortex. J. Neurosci. 2005; 25:3962–3972. [PubMed: 15829648]
59. Palva S, Palva JM. Discovering oscillatory interaction networks with M/EEG: challenges and breakthroughs. Trends Cogn Sci. 2012; 16(4):219–230. [PubMed: 22440830]
60. Pascual-Marqui RD. Instantaneous and lagged measurements of linear and non linear dependence between groups of multivariate time series: frequency. 2007 arXiv:0711.1455 [stat.ME] 2007 November, http://arxiv.org/abs/0711.1455.
61. Pascual-Marqui RD, Biscay RJ, Valdes-Sosa P, Bosch-Bayard J, Riera-Diaz JJ. Cortical current source connectivity by means of partial coherence fields. 2011 arXiv:1108.0251v1 [stat.AP] 2011 August http://arxiv.org/abs/1108.0251v1.
62. Romei V, Gross J, Thut G. On the role of prestimulus alpha rhythms over occipito-parietal areas in visual input regulation: correlation or causation? J. Neurosci. 2010; 30:8692–8697. [PubMed: 20573914]
63. Rushworth MF, Krams M, Passingham RE. The attentional role of the left parietal cortex: the distinct lateralization and localization of motor attention in the human brain. J Cogn Neurosci. 2001; 13:698–710. [PubMed: 11506665]
64. Schnitzler A, Gross J. Functional connectivity analysis in magnetoencephalography. International review of neurobiology. 2005; 68:173–195. [PubMed: 16443014]
65. Schoffelen JM, Gross J. Source connectivity analysis with MEG and EEG. Human Brain Mapping. 2009; 30:1857–1865. [PubMed: 19235884]
66. Sekihara K, Nagarajan SS, Poeppel D, Marantz A, Miyashita Y. Reconstructing spatio-temporal activities of neural sources using an MEG vector beamformer technique. IEEE Trans. Biomed. Eng. 2001; 48:760–771. [PubMed: 11442288]
67. Sekihara K, Nagarajan SS, Poeppel D, Marantz A. Asymptotic SNR of scalar and vector minimum-variance beamformers for neuromagnetic source reconstruction. IEEE Trans. Biomed. Engin. 2004; 51(10)
68. Sekihara K, Owen JP, Trisno S, Nagarajan SS. Removal of spurious coherence in MEG source-space coherence analysis. IEEE Trans Biomed Eng. 2011; 58:3121–3129. [PubMed: 21824842]
69. Siegel M, Donner TH, Oostenveld R, Fries P, Engel AK. Neuronal synchronization along the dorsal visual pathway reflects the focus of spatial attention. Neuron. 2008; 60(4):709–719. [PubMed: 19038226]

70. Siegel M, Donner TH, Engel AK. Spectral fingerprints of large-scale neuronal interactions. Nat.Rev.Neurosci. 2012; 13:121–134. [PubMed: 22233726]
71. Smith SM, Bandettini PA, Miller KL, Behrens TE, Friston KJ, David O, Liu T, Woolrich MW, Nichols TE. The danger of systematic bias in group-level FMRI-lag-based causality estimation. NeuroImage. 2012; 59:1228–1229. [PubMed: 21867760]
72. Snyder AC, Foxe JJ. Anticipatory attentional suppression of visual features indexed by oscillatory alpha-band power increases: a high-density electrical mapping study. J Neurosci. 2010; 30:4024–4032. [PubMed: 20237273]
73. Stam CJ, Nolte G, Daffertshofer A. Phase lag index: assessment of functional connectivity from multi channel EEG and MEG with diminished bias from common sources. Hum. Brain Mapp. 2007; 28:1178–1193. [PubMed: 17266107]
74. Tallon-Baudry C, Bertrand O, Delpuech C, Pernier J. Stimulus specificity of phase-locked and non-phase-locked 40 Hz visual responses in human. J Neurosci. 1996; 16:4240–4249. [PubMed: 8753885]
75. Thut G, Nietzel A, Brandt SA, Pascual-Leone A. Alpha-band electroencephalographic activity over occipital cortex indexes visuospatial attention bias and predicts visual target detection. J Neurosci. 2006; 26:9494–9502. [PubMed: 16971533]
76. Tsai AC, Liou M, Jung TP, Onton JA, Cheng PE, Huang CC, Duann JR, Makeig S. Mapping single-trial EEG records on the cortical surface through a spatiotemporal modality. Neuroimage. 2006; 32:195–207. [PubMed: 16730194]
77. Ugurbil K. The road to functional imaging and ultrahigh fields. NeuroImage. 2012; 62:726–735. [PubMed: 22333670]
78. van Ede F, de Lange F, Jensen O, Maris E. Orienting attention to an upcoming tactile event involves a spatially ad temporally specific modulation of sensorimotor alpha- and beta-band oscillations. J. Neurosci. 2011; 31:2016–2024. [PubMed: 21307240]
79. Van Essen DC, Dickson J, Harwell J, Hanlon D, Anderson CH, Drury HA. An Integrated Software System for Surface-based Analyses of Cerebral Cortex. Journal of American Medical Informatics Association. 2001; 8:443–459.
80. Varela F, Lachaux J, Rodriguez E, Martinerie J. The brain web: phase synchronization and large-scale integration. Nat Rev Neurosci. 2001; 2:229–239. [PubMed: 11283746]
81. Vinck M, Oostenveld R, van Wingerden M, Battaglia F, Pennartz CM. An improved index of phase-synchronization for electrophysiological data in the presence of volume-conduction, noise and sample-size bias. NeuroImage. 2011; 55:1548–1565. [PubMed: 21276857]
82. Wang L, Saalmann YB, Pinsk MA, Arcaro MJ, Kastner S. Electrophysiological low-frequency coherence and cross-frequency coupling contribute to BOLD connectivity. Neuron. 2012; 76:1010–1020. [PubMed: 23217748]
83. Womelsdorf T, Schoffelen JM, Oostenveld R, Singer W, Desimone R, Engel AK, Fries P. Modulation of Neuronal Interactions Through Neuronal Synchronization. Science. 2007; 316(5831):1609–1612. [PubMed: 17569862]
84. Worden MS, Foxe JJ, Wang M, Simpson GV. Anticipatory biasing of visuospatial attention indexed by retinotopically specific alpha-band electroencephalography increases over occipital cortex. J Neurosci. 2007; 20:RC63. [PubMed: 10704517]
85. Yeo BT, Krienen FM, Sepulcre J, Sabuncu MR, Lashkari D, Hollinshead M, Roffman JL, Smoller JW, Zollei L, Polimeni JR, Fischl B, Liu H, Buckner RL. The Organization of the Human Cerebral Cortex Estimated By Functional Connectivity. J Neurophysiol. 2011; 106:1125–1165. [PubMed: 21653723]

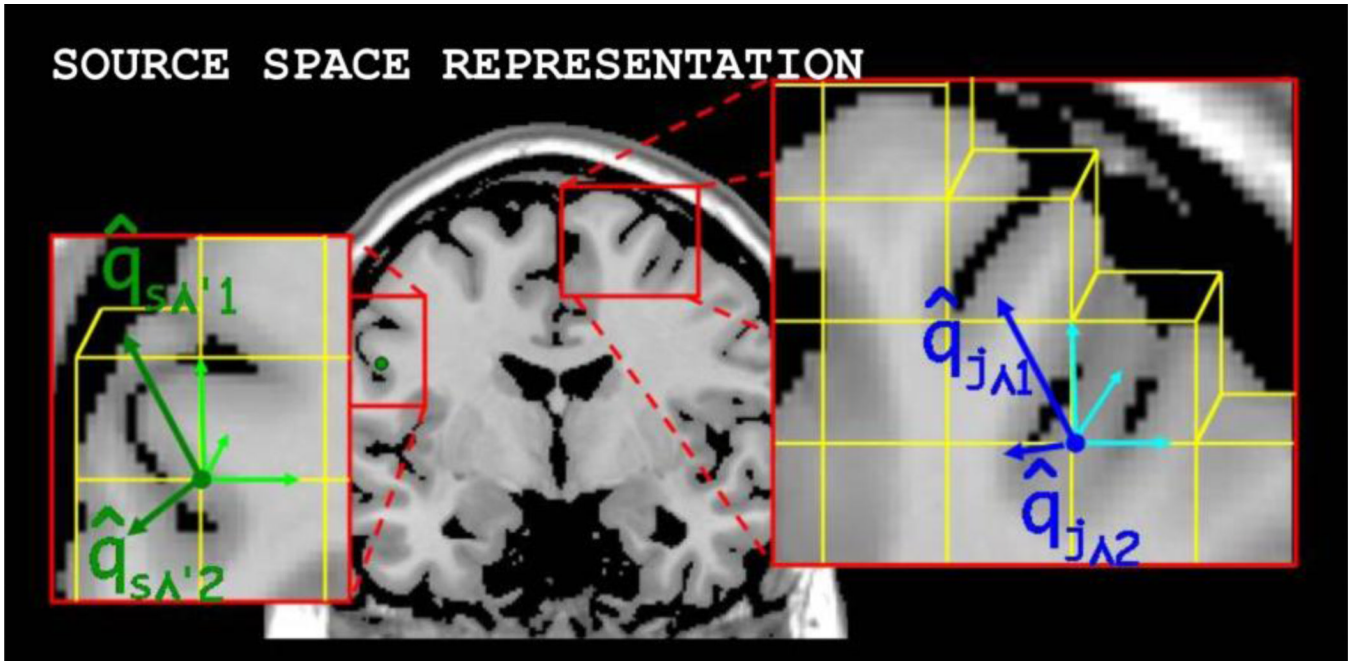

Figure 1.
Schematic illustration of the 3D grid source space signal components before and after principal component analysis.

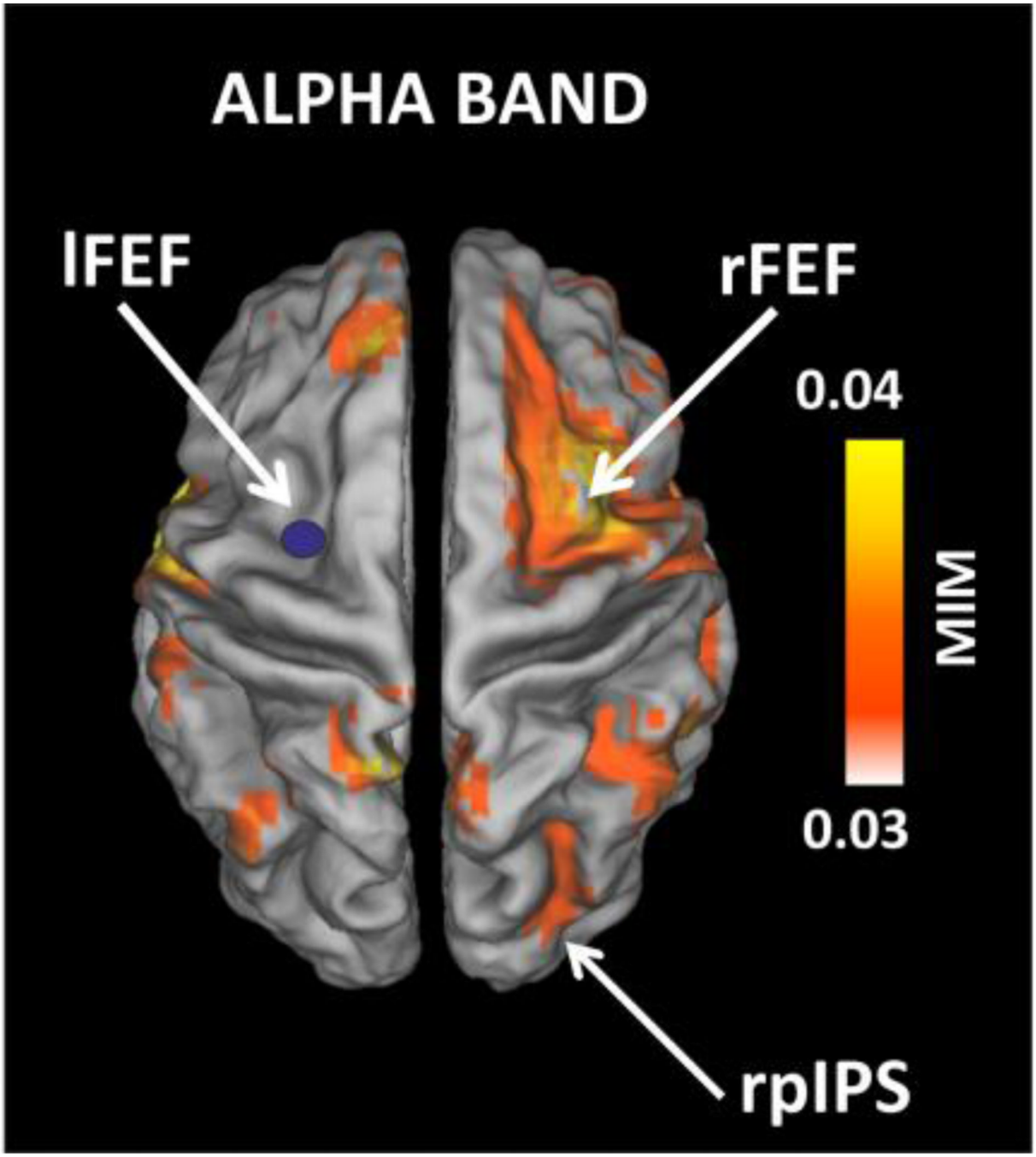

Figure 2.
Whole brain map of the MIM values in the alpha frequency band for the left FEF seed. This map is thresholded above the statistically significant level. The seed location is marked by a blue dot and the network node locations are marked by white arrows and labeled in accordance with the coordinates listed in Table 1.

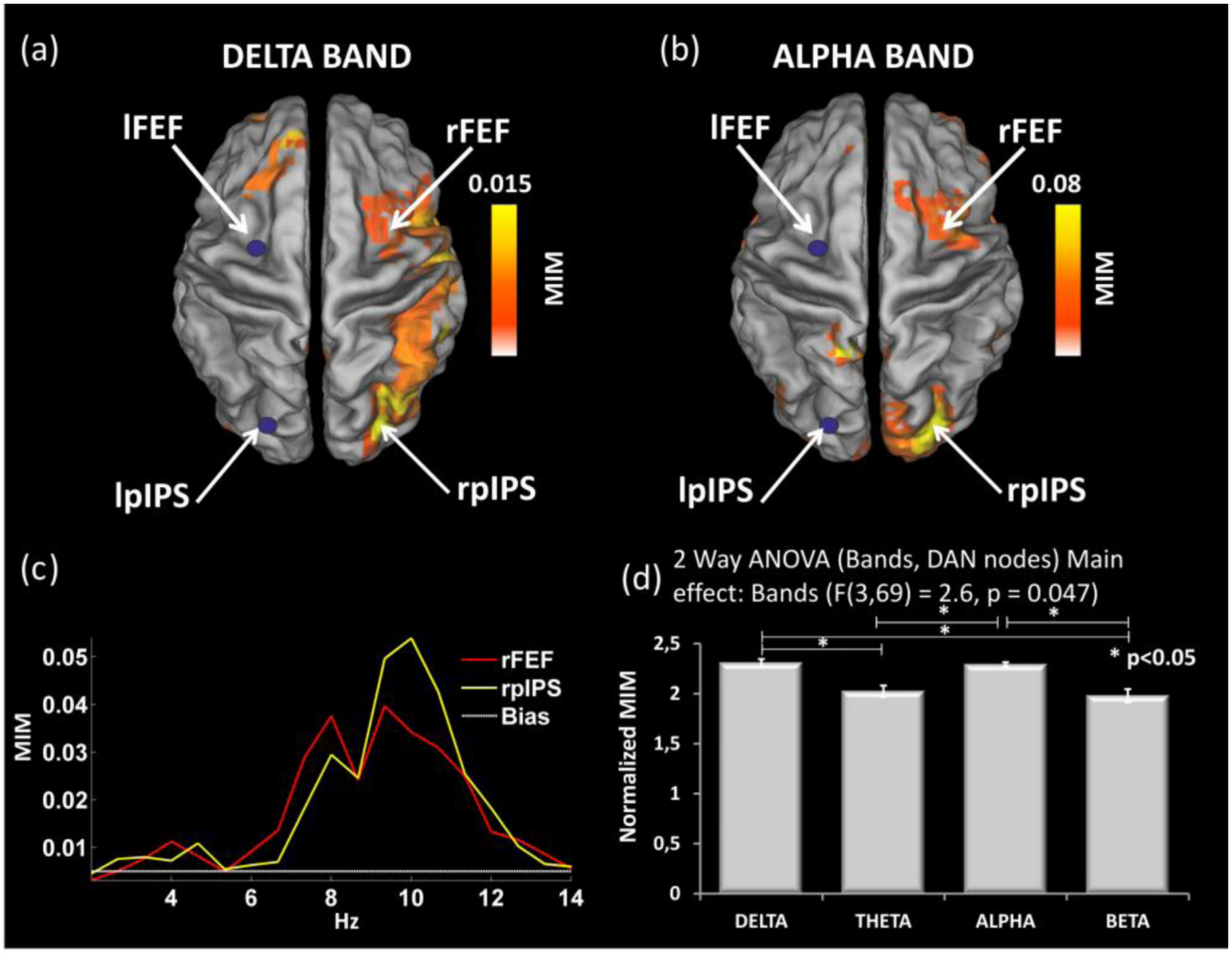

Figure 3.

(a, b) Whole brain left FEF and PIPS conjunction maps of MIM values in delta and alpha frequency bands. These maps reveal out of phase interactions between the seeds and DAN nodes in the contralateral hemisphere. This interaction is frequency specific, as shown by the plot as a function of frequency (c). The seed locations are marked by a blue dot and the network node locations are marked by white arrows and labeled in accordance with the coordinates listed in Table 1. (d) Post-hoc results for the 2-WAY ANOVA with factors Frequency Bands and DAN Nodes ($F(3,69)=2.6$, $p=0.047$) for MIM values. The main effect concerns Frequency Bands: MIM values within-DAN in the alpha and delta bands are statistically significantly greater than those in theta and beta.

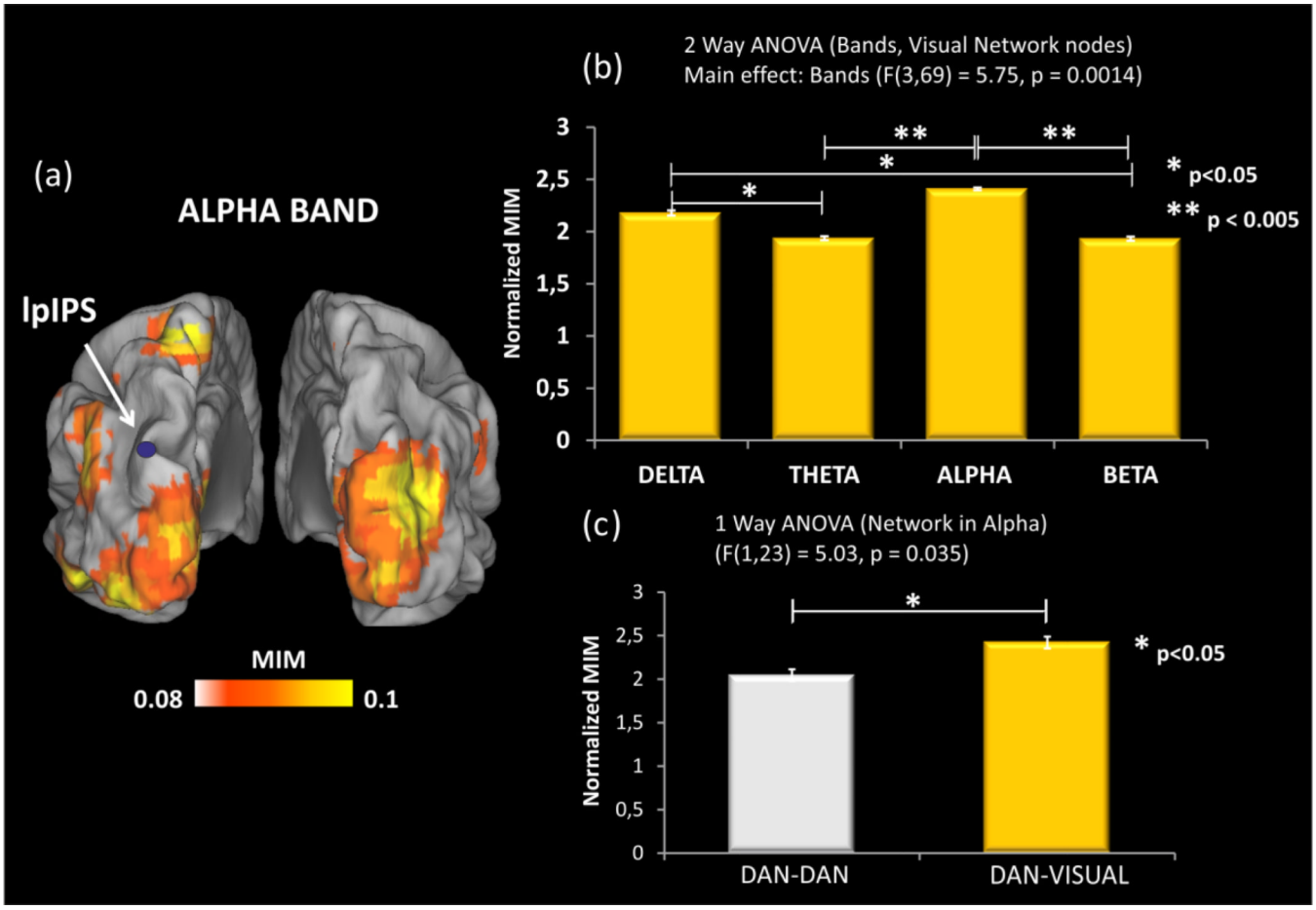

Figure 4.

(a) Whole brain left FEF and PIPS conjunction map of the MIM values in the alpha band. The left pIPS seed location is marked by a blue dot whereas the left FEF seed is out of the field of view. This map reveals alpha band specific out of phase interaction between the DAN seeds and visual network nodes in both hemispheres. (b) Post-hoc results for the 2-WAY ANOVA with factors Frequency Bands and Visual Network Nodes ($F(3,69)=5.75$, $p=0.0014$) for MIM values. The main effect concerns Frequency Bands: MIM for across-network interaction between DAN and Visual Network in the alpha band are statistically significantly greater than those theta and beta. (c) Post-hoc results for the 1-WAY ANOVA with factor Node ($F(1,23)=5.03$, $p=0.035$) of MIM values in the alpha frequency band from DAN and Visual Network nodes. MIM values for the average of Visual Network nodes are significantly greater than those within the dorsal attention network for the average of right FEF and right pIPS in alpha.

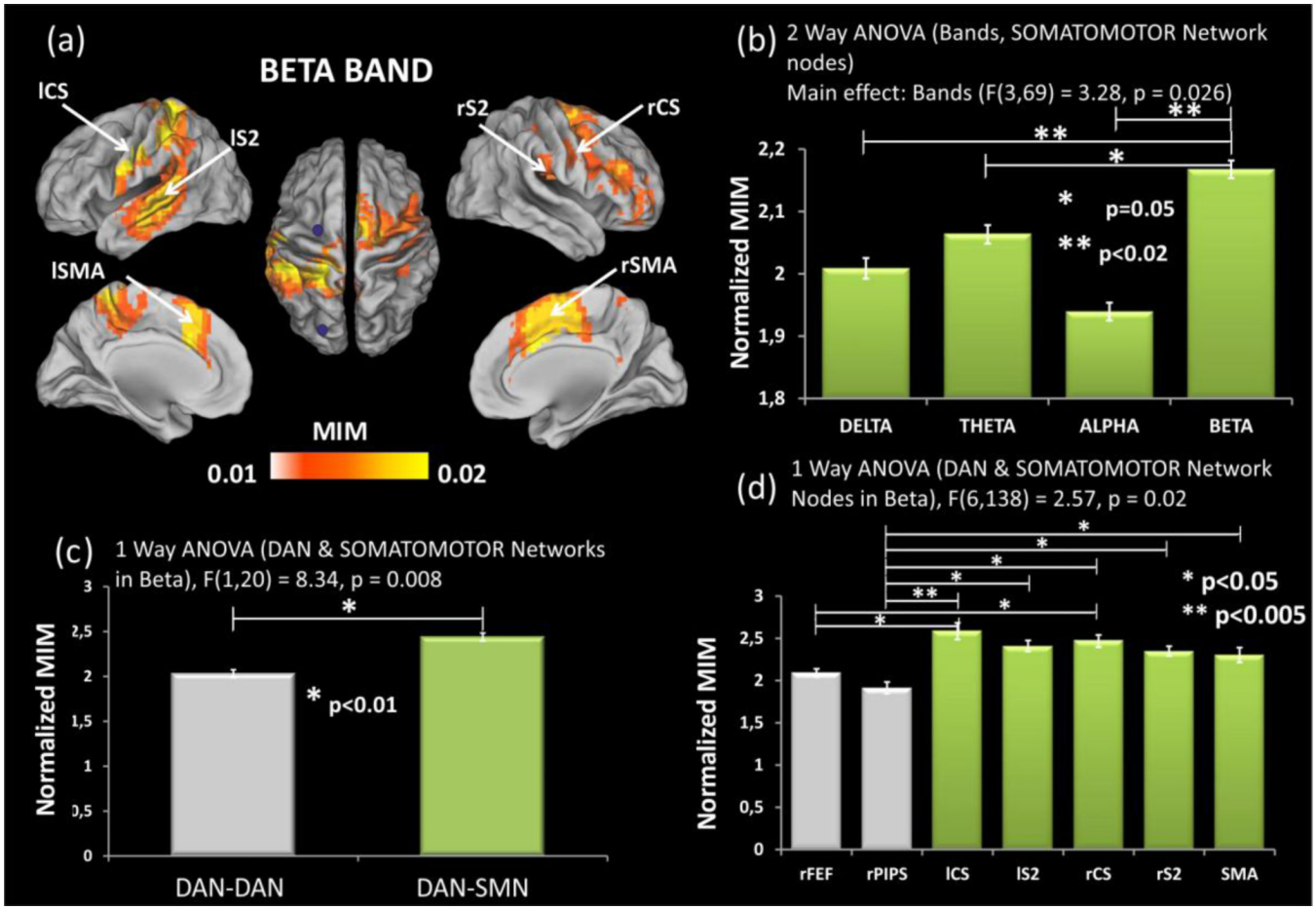

Figure 5.

(a) Whole brain left FEF and PIPS conjunction map of the MIM values in beta band. This map reveals beta band specific out of phase interaction between the DAN seeds and Somatomotor Network nodes in both hemispheres. Specifically, left central sulcus (lCS), secondary somatosensory areas (lS2) and supplementary motor area (lSMA), secondary somatosensory areas (rS2) and supplementary motor area (rSMA) are involved in this interaction. (b) Post-hoc results for the 2-WAY ANOVA with factors Frequency Bands and Somatomotor Network Nodes ($F(3,69)=3.28$, $p=0.026$) for MIM values. The main effect concerns Frequency Bands: the MIM for “across” network interaction between DAN and Somatomotor Network in the beta band are significantly greater than those in delta and alpha. (c) Post-hoc results for the 1-WAY ANOVA with factor DAN and Somatomotor Network Nodes ($F(1,20)=8.34$, $p=0.008$) for beta band MIM. MIM averaged across Somatomotor Network nodes (lCS, lS2, lSMA, rCS, rS2 and rSMA) is significantly greater than than similarly averaged MIM in right hemisphere DAN nodes. (d) Post-hoc results for the 1-WAY ANOVA with factor DAN and Somatomotor Network Nodes ($F(6,138)=2.75$, $p=0.02$) for MIM values in the beta frequency band. Here, each node is considered individually. MIM values in all Somatomotor Network nodes (lCS, lS2, lSMA, rCS, rS2 and rSMA) were significantly greater than those in the right pIPS; MIM in lCS and rCS also were greater than MIM in rFEF. Seed locations are marked by a blue dot and the network node locations are marked by white arrows and labeled in accordance with the coordinates listed in Table 1.

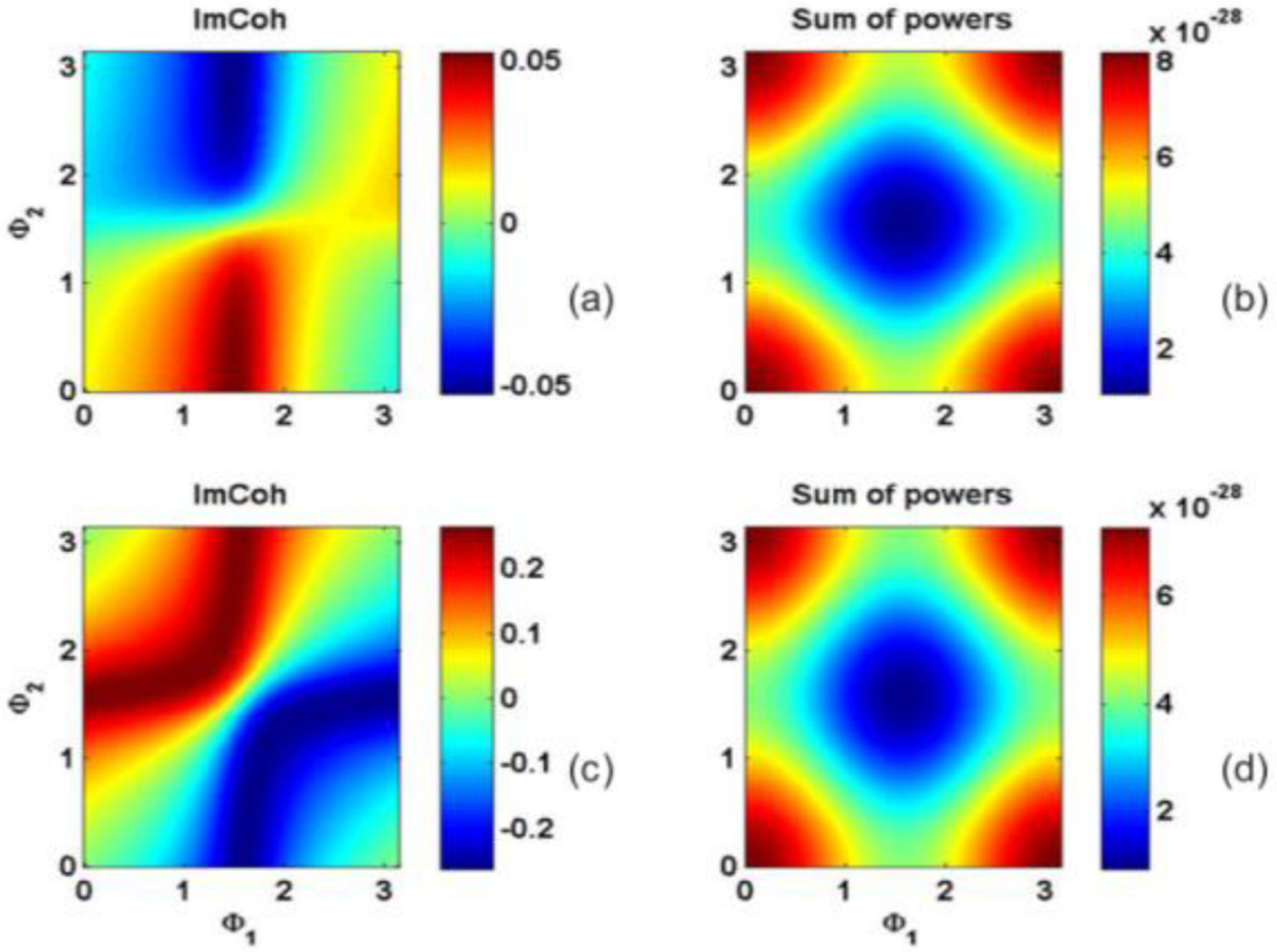

Figure 6.

Imaginary part of coherence (ImCoh) and sum of powers for two dipoles the directions of which are indicated by the angles Φ_1 and Φ_2, respectively. Each direction varies in the range [0, π]. Two different situations are presented: dipoles located in distant voxels (top row, panels a and b), dipoles located at the same voxel (bottom row, panels c and d). In more detail we show: (a) ImCoh for dipole located in distant voxels (left and right motor areas); (b) sum of powers for the same situation shown in (a); (c) ImCoh for dipole located at the same voxel; (d) sum of powers for the same situation shown in (c).

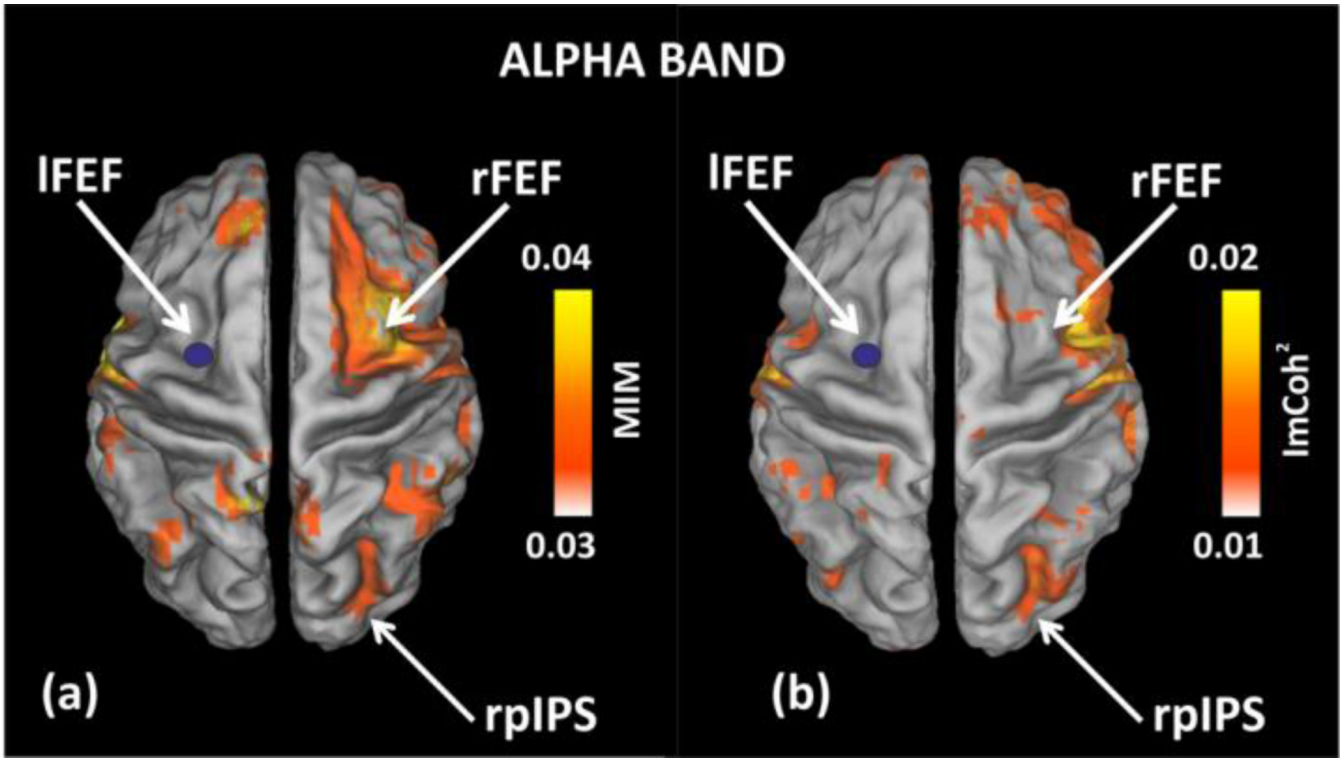

Figure 7.
(a) MIM map in the alpha band obtained by seeding lFEF (same of Figure 2); (b) squared imaginary coherence map obtained by seeding lFEF and calculated from the first principal direction only (scalar analogous of (a)).

Table 1

Node coordinates for Dorsal Attention, Somatomotor and Visual Networks in MNI space. DAN seed coordinates are highlighted in yellow in the first two rows.

NETWORK	ROI label	MNI coordinates [x, y, z]
Dorsal Attention Network	lFEF	[−26, −12, 53]
Dorsal Attention Network	lPIPS	[−25, −67, 48]
Dorsal Attention Network	lVIPS	[−24, −73, 29]
Dorsal Attention Network	rFEF	[30, −13, 53]
Dorsal Attention Network	rPIPS	[23, −69, 49]
Dorsal Attention Network	rVIPS	[30, −83, 13]
Somato-motor Network	lCS	[−32, −36, 55]
Somato-motor Network	lS2	[−39, −27, 18]
Somato-motor Network	lSMA	[−1, −17, 55]
Somato-motor Network	rCS	[32, −35, 58]
Somato-motor Network	rS2	[36, −23, 21]
Somato-motor Network	rSMA	[4, −15, 52]
Visual Network	lV1	[−2, −99, −3]
Visual Network	lV2v	[−5, −77, −11]
Visual Network	lV3	[−8, −96, 10]
Visual Network	lV4	[−29, −76, 18]
Visual Network	rV1v	[10, −91, 3]
Visual Network	rV2d	[14, −95, 10]
Visual Network	rV3	[18, −94, 15]